Additive manufacturing for Powering the Blue Economy applications: A tidal turbine blade case study

M. González-Montijo, P. Murdy, C. Candon, R. Beach, C. Nichols, and P. Barden

Abstract— **As the marine renewable energy industry continues to expand, innovation in the manufacturing space must grow accordingly to reduce costs and ensure the economic feasibility of new technologies. Additive manufacturing, more commonly known as 3D printing, provides an alternative for rapid prototyping of marine hydrokinetic technologies, particularly supporting Powering the Blue Economy™ initiatives of the U.S. Department of Energy Water Power Technologies Office. This study explores the application of additive manufacturing in the development of marine hydrokinetic structures, focusing on material and printing method selection, design, and analysis of a 3D-printed spar for an axial-flow tidal turbine blade. Corrosion-resistant metals were deemed ideal due to the loads and harsh marine environment the blade would experience. Laser metal deposition methods were determined to be the most effective and scalable for the considered scale. The designed spar adapts its geometry to the blade—a feature uniquely suited to additive manufacturing—and is intended to serve as the blade's primary structural component. A finite element model was used to study stresses and deformations under loading conditions. The spar was manufactured using 316L stainless steel through direct energy deposition, and defects were assessed and recorded. Future efforts will include mechanical testing of the spar. This research establishes a benchmark process for using additive manufacturing in developing marine hydrokinetic structures, paving the way for future optimization and techno-economic analysis.**

Keywords—**Additive manufacturing, laser metal deposition, structural design, tidal energy.**

I. Introduction

The pressing need for clean energy sources has never been more apparent, as global communities face the immense challenge of mitigating climate change and transitioning to a sustainable future. Marine renewable energy (MRE) has emerged as a promising clean energy source in recent years, aiming to harness the vast potential of the world's oceans to generate power with minimal environmental impact. As global interest in tapping into the power of the oceans continues to grow, recent advancements in tidal energy technologies have resulted in remarkable innovations, heralding a bright future for MRE.

In response, the U.S. Department of Energy Water Power Technologies Office launched the Powering the Blue Economy™ (PBE) initiative, which is targeted at understanding and aiding in the energy needs of emerging maritime markets and coastal communities and ensuring their sustainable growth. This initiative aims to catalyze the growth and development of MRE by fostering innovations in materials and manufacturing processes, thereby enhancing the economic viability of tidal energy solutions [1]. By supporting research and development in this area, the PBE initiative seeks to accelerate the adoption of MRE technologies and contribute to the global transition toward clean energy technologies.

One of the key areas of research in the MRE space is the development of efficient and cost-effective manufacturing processes for marine hydrokinetic (MHK) turbine blades. Additive manufacturing (AM), also known as 3D printing, has emerged as a particularly promising technology in this

This work was authored by the National Renewable Energy Laboratory, operated by Alliance for Sustainable Energy, LLC, for the U.S. Department of Energy (DOE) under Contract No. DE-AC36-08GO28308. Funding provided by the U.S. Department of Energy Office of Energy Efficiency and Renewable Energy Water Power Technologies Office. The views expressed in the article do not necessarily represent the views of the DOE or the U.S. Government. The U.S. Government retains and the publisher, by accepting the article for publication, acknowledges that the U.S. Government retains a nonexclusive, paid-up, irrevocable, worldwide license to publish or reproduce the published form of this work, or allow others to do so, for U.S. Government purposes.

M. Gonzalez-Montijo is with the University of Washington, Seattle WA, USA (email: gonzam8@uw.edu)

P. Murdy, C. Candon, R. Beach, and C. Nichols are with the National Renewable Energy Laboratory, 15013 Denver West Parkway, Golden, CO 80401, USA

P. Barden is with Ai-Build, Unit D1, Leyton Industrial Village, London, E10 7QP, UK

Digital Object Identifier: https://doi.org/10.36688/ewtec-2023-420

Fig. 1. A computational rendering of the MHKF1 turbine with 2.5 m rotor diameter (image credit to Sandia National Laboratories).

regard [2]. Aside from its capacity to produce complex geometries, AM also offers other significant advantages, such as reduced material waste, shortened production times, and enhanced design flexibility. This technology has also evolved to accommodate a diverse range of materials, from polymers to metals, increasing its versatility [3].

Although AM has shown great potential in various industries, its application in marine energy technologies is still an emerging field, with ample room for growth and optimization. As AM continues to mature, it is expected to play an increasingly important role in the advancement of MRE and contribute to the development of next-generation MHK turbine blades. To demonstrate the potential of AM for MRE applications, it is essential to conduct research that produces benchmark 3D-printed MHK structures. By modeling, developing, and validating these structures, researchers can demonstrate the feasibility and effectiveness of AM as a manufacturing process for MRE technologies. The foundational work presented herein not only paves the way for further optimization and innovation in the field but also helps build confidence in the adoption of AM techniques for the MRE industry.

The primary goal of this project was to explore a small-scale tidal turbine project as a case study for AM and to identify suitable AM processes and materials. Specifically, the project aimed to design, model, develop, and manufacture a 3D-printed structural spar for an axial-flow tidal turbine blade. This spar is based on a reference tidal turbine blade design (named MHK-Family 1, or MHKF1) resulting from a joint effort between Sandia National Laboratories (Sandia), the University of California, Davis, and the Applied Research Lab at Penn State University [4]. By investigating the feasibility of AM in this context, this research aimed to contribute valuable insights to the ongoing development of MRE technologies and manufacturing processes.

The MHKF1 turbine is currently being developed and constructed by Sandia and the University of New Hampshire (UNH) for deployment at the UNH Tidal Energy Test Site at Memorial Bridge in New Hampshire as part of a loads measurement campaign. It will have a 2.5 m diameter rotor (see Fig. 1) with a rated power of 25 kW [5]. The blades themselves are 1.05 m long and incorporate several novel design features to reduce cavitation, erosion, and noise generation. They are designed to optimize power performance through a wider range of tip-speed ratios.

II. MATERIAL AND MANUFACTURING PROCESS SELECTION

A. *Loading analysis*

Before determining the optimal AM processes and materials for the MHKF1 blade spar design, an initial understanding of the operating environment and design loads was required. Using an inflow speed of 3 m/s, performance outputs for the MHKF1 turbine were modeled using OpenFAST for a range of rotational speeds and tip-speed ratios. These efforts, which are to be further discussed in a separate publication, yielded the worst-case tip-speed ratios and rotational velocities (5.58 and 130 rpm) in terms of thrust loading. These were then used to

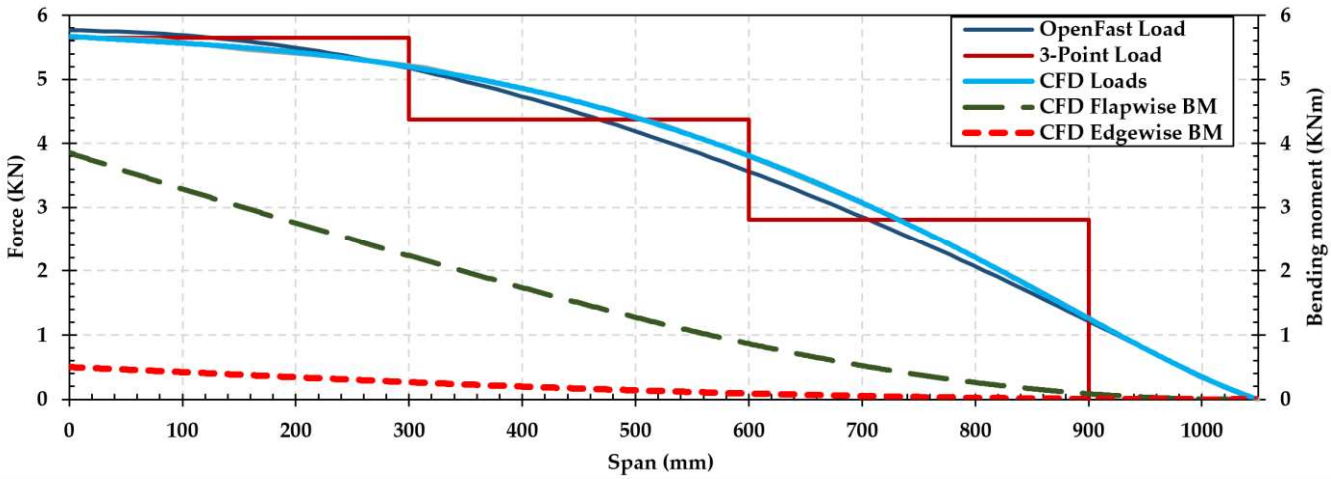

Fig. 2. Flapwise and edgewise shear forces and bending moments derived from surface pressure distributions from the static CFD analysis.

TABLE I
THE AM PROCESS DECISION MATRIX WITH BILLET MACHINING AS THE REFERENCE MANUFACTURING PROCESS

Requirements	Weight	Billet Machining	FDM	DED
Capital cost	3	-1	2	1
Deposition rate	2	0	2	1
Surface finish	3	1	-1	-1
Resolution	1	1	0	-1
Post-processing	3	2	0	0
Material options	2	1	1	2
Porosity	1	2	-2	2
Ease of feature integration	2	-1	2	1
Scalability (size)	4	0	2	2
Scalability (performance)	3	1	1	2
Accessibility	2	2	2	1
Total score		16	26	25

build a static computational fluid dynamics (CFD) model of a single rigid blade to determine pressure distributions across the full outer surface of the blade. The pressure distributions were then applied to a finite element model of the full blade geometry to extrapolate simplified bending moment and shear force distributions in the flapwise (thrust) and edgewise (rotational) directions (see Fig. 2). Only static loads were determined. Fatigue loads require a much more extensive numerical modeling effort, which was beyond the scope of this research project.

Section III will outline how these loading distributions were utilized to design and analyze the final blade spar structure. However, the maximum root bending moments and shear forces, 3.9 kN·m and 5.6 kN, respectively, were considerably high for a 1.05 m blade. It was an indication that high-strength and high-modulus materials would be required to sustain the hydrodynamic loads reliably, even if the blade was to be 3D-printed as a single solid component.

B. *Additive manufacturing process selection*

To determine the ideal AM processes for producing the MHKF1 blade, a decision matrix approach was taken. Key criteria for the manufacturing of the blade were given weights in terms of importance, ranging from 0 to 4. A variety of AM processes were scored from -2 to 2 for each criterion. Some scores were determined by ranking known parameters (such as deposition rate), whereas others required a degree of subjectivity, driven by informed judgement and contextual considerations. Total scores were calculated as the sum of the criteria weight multiplied by the individual criteria scores. Since the actual MHKF1 blade structures, designed by Sandia and UNH, are to be CNC-machined from billet aluminum, this process was also included in the decision matrix.

Table I illustrates this process and shows the scores for the most highly ranked AM processes: fused deposition modeling (FDM) and directed energy deposition (DED). Many other AM processes, such as stereolithography, selective laser sintering, and binder jet were evaluated but were omitted for brevity.

FDM and DED were primarily chosen as top candidates due to their scalability (in both size and performance) and the available materials for those processes. Section II-C provides more detail on available materials for those processes.

C. *Material selection*

Like the AM processes, AM materials were downselected using a decision matrix approach. Table II shows the critical material requirements. Aluminum is also included as comparative reference material. Table II also shows the process/material combined totals, calculated as the sum of the AM process and material scores.

Many materials are available for FDM and DED manufacturing processes. For example, FDM materials are typically polymers ranging from Acrylonitrile butadiene styrene (ABS) to nylon, with and without chopped or continuous fiber reinforcements for enhanced mechanical properties. DED processes can use many different metal alloys that are available as wire feedstock.

TABLE II
THE AM MATERIAL DECISION MATRIX WITH ALUMINIUM AS THE REFERENCE MATERIAL

Requirements	Weight	Machining – Aluminium 6061-T6	FDM – Chopped Carbon ABS	FDM – Ultem (polyetherimide)	DED – 316L Stainless Steel	DED – Ti-6Al-4V
Static strength	3	1	-1	-1	1	2
Fatigue strength	3	0	1	1	1	1
Elastic modulus	4	0	-1	-1	2	1
Density	1	0	2	2	-2	-1
Environmental resistance	4	1	2	2	1	2
UV resistance	2	2	-1	2	2	2
Toughness	3	2	0	0	2	1
Cost	2	-1	2	1	1	-2
Total score		15	9	12	25	23
Combined process/material score		31	35	38	50	48

TABLE III
MHKF1 AND SPAR GEOMETRIC PROPERTIES THROUGHOUT THE BLADE SPAN

Span [mm]	Twist [deg]	Chord [mm]	Spar Width [mm]	Chord [%]	Wall Thickness [mm]
0	47.9	210.2	125	59.50%	6
78.66	37.8	256.59	120	46.80%	6
157.3	32	306.35	115	37.50%	6
209.9	27.9	294.91	110	37.30%	5
262.5	24.5	278.89	105	37.60%	5
315.1	21.4	259.93	100	38.50%	5
367.6	18.7	243.16	95	39.10%	5
420.2	16.3	224.25	90	40.10%	5
472.8	14.1	207.41	85	41.00%	5
525.4	12.3	192.5	80	41.60%	5
577.9	10.9	179.25	75	41.80%	5
630.5	9.82	167.41	70	41.80%	5
683.1	8.89	156.73	65	41.50%	4
735.7	8.1	146.99	60	40.80%	4
788.3	7.27	137.91	55	39.90%	4
840.8	6.6	129.15	50	38.70%	4
893.4	5.92	120.22	45	37.40%	3
946	5.21	110.1	40	36.30%	3
998.6	4.52	96.26	30	31.20%	2
1050	3.59	56.48	20	35.40%	2

Like Table I, Table II does not show all the materials that were evaluated. Key criteria of importance for the chosen materials were static and fatigue strengths, elastic modulus, environmental and corrosion resistance, and toughness.

The overall results presented in Table II led the team to the conclusion that a component-based, multi-AM process, multimaterial approach would be taken for the 3D-printed MHKF1 blade demonstration. The main structural component was to be a box spar made of 316L stainless steel (SS) using DED due to the superior strengths and moduli of metal materials [6–10]. The remaining leading- and trailing-edge hydrodynamic fairings would be manufactured using FDM with either chopped carbon ABS or Ultem, due to their good resistance to environmental degradation and the low-cost and high deposition rates of FDM machines. The proceeding sections of this manuscript will only focus on the design and manufacturing of the structural box spar because it is the more complex and critical component.

III. STRUCTURAL DESIGN APPROACH

The spar design approach undertaken in this study both follows and supports a slightly modified version of the MHKF1 blade as observed in Fig. 3. This geometry is part of a 2.5 m diameter three-bladed marine turbine rotor assembly [4]. This section will detail how specific geometric details and loading distributions of the modified MHKF1 blade were used to inform the design and analysis of the final blade structure. Notably, high root bend moments and shear forces, 3.9 kN·m and 5.6 kN, respectively, established early on the need for high-strength and high-modulus materials to reliably sustain the hydrodynamic loads, even when considering the possibility of 3D-printing the blade as one solid component.

Fig. 3. Geometric definition of structural spar within the MHKF1 blade.

TABLE IV
316L SS MECHANICAL PROPERTIES IN THE OUT-OF-PLANE DIRECTION

Material	Yield Strength [MPa]	Elastic Modulus [MPa]	Density [kg/m^3]
316L Stainless Steel	300	190000	8000

A. *Geometric analysis and design*

The MHKF1 blade design, the basis for our study, is defined from root to tip by 20 unique hydrofoil cross sections. Each section carries its own distinct geometry, twist, and chord length. As demonstrated in Table III, the blade twist and chord length vary significantly across the blade span. This variability introduces complexity to the design-for-manufacturing process, making the geometry particularly well-suited to AM methods that can easily accommodate such intricacies.

The design of the blade's structural spar was established considering the low- and high-pressure surfaces, as well as the aerodynamic center of the blade, located approximately 30% of the chord length from the leading edge. Once the top and bottom faces of the spar were set to align with the blade surfaces, three parameters were left to explore: width, wall thickness, and chordwise location.

Beginning with the assumption of a spar with a basic hollow square cross section, a MATLAB function was developed to determine minimum wall thicknesses, t, at any given point, i, at various locations along the blade by solving for t_i in Eq. (1). This equation takes a simple mechanics of materials approach to bending stresses in cantilever beams. The function used the material yield stress, σ_y, a chosen safety factor, n, the spar width at a given spanwise point, w_i, (determined as a fraction of chord length), the hydrofoil thickness at a given point, h_i, and the bending moment at a given spanwise location, M_i, as depicted in Fig. 2.

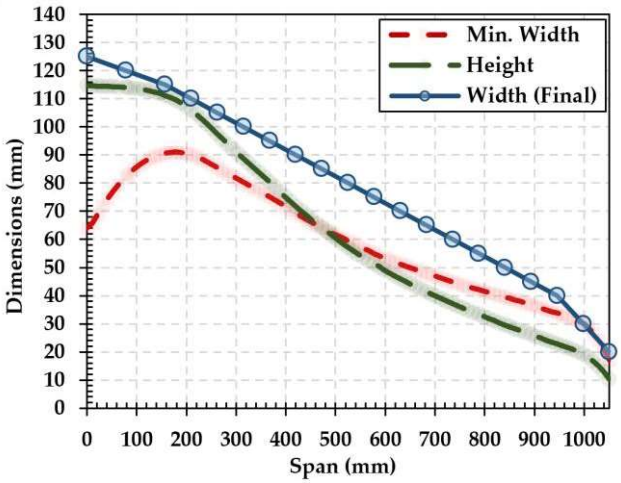

Fig. 4. Spar spanwise geometric dimensions.

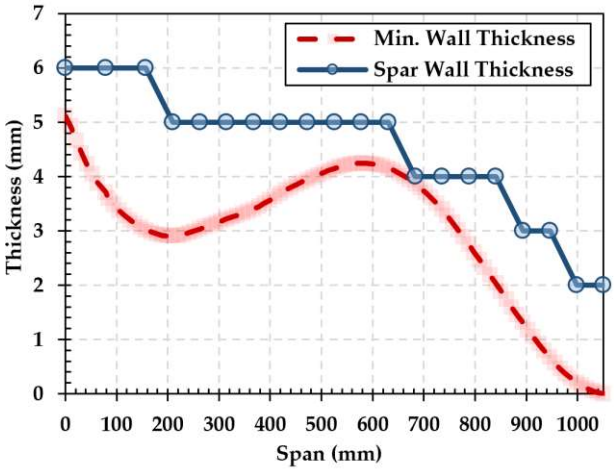

Fig. 5. Spar spanwise wall thicknesses calculated by the MATLAB function.

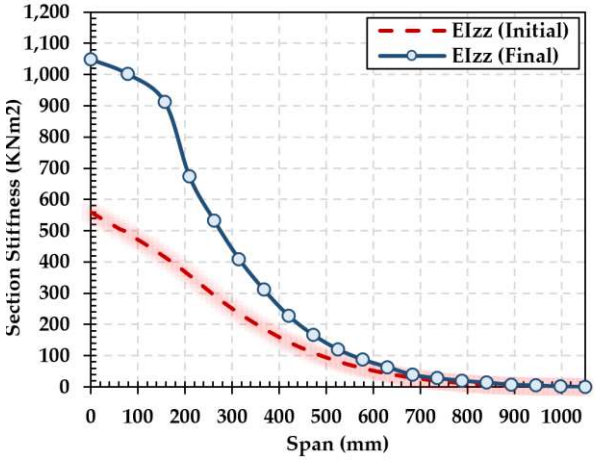

Fig. 6. Calculated cross-sectional stiffnesses from the MATLAB function.

$$\sigma_y = \frac{6nM_i h_i}{w_i(h_i^3 - (h_i - t_i)^3)} \quad (1)$$

The chosen material for the spar was 316L SS. Due to the anisotropic nature of 3D-printed materials, the mechanical properties were taken as the lowest ones provided by

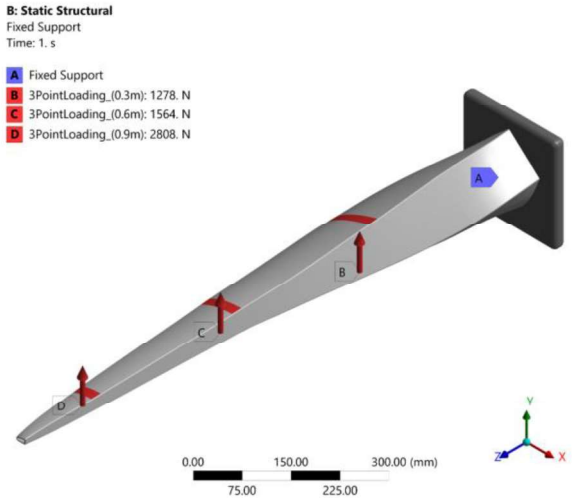

Fig. 7. Spar finite element analysis setup: loads and boundary conditions.

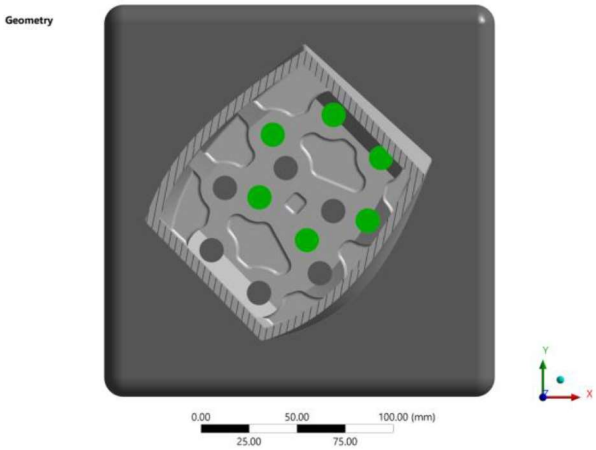

Fig. 8. Spar cross-sectional cut: interior root design. Bolts considered in analysis are highlighted in green.

Meltio's datasheets (the XZ out-of-plane direction) and are shown in Table IV. These properties provided a robust starting point for the design, as well as a safety factor of 4 and a minimum width of 30% chord length. Given that the spar would not retain a perfectly rectangular shape due to the need to follow the low- and high-pressure surfaces, a more conservative and practical approach was adopted for the final design. Fig. 4-6 displays the minimum required spanwise width, wall thickness, and section stiffness juxtaposed with the final chosen design parameters.

The development of the spar's root section was carried out with particular care, ensuring it was compatible with the hub mounts of the turbine, which are positioned at 50% chord. To provide greater flexibility in structural testing setup, the design incorporated dual hexagonal 6-bolt patterns, overlaid in such a way as to enable the spar to connect to the rotor at both 50% and 30% of the root chord. These bolt patterns were tailored to accommodate ½" fasteners. In order to reinforce the area surrounding the bolts, ensure effective torque load transfer to the turbine, and guarantee at least 1.5 diameters of thread engagement for each fastener, a root plate thickness of 10 mm was selected, along with an additional 10 mm extrusion surrounding the bolts. This approach led to longer bolt

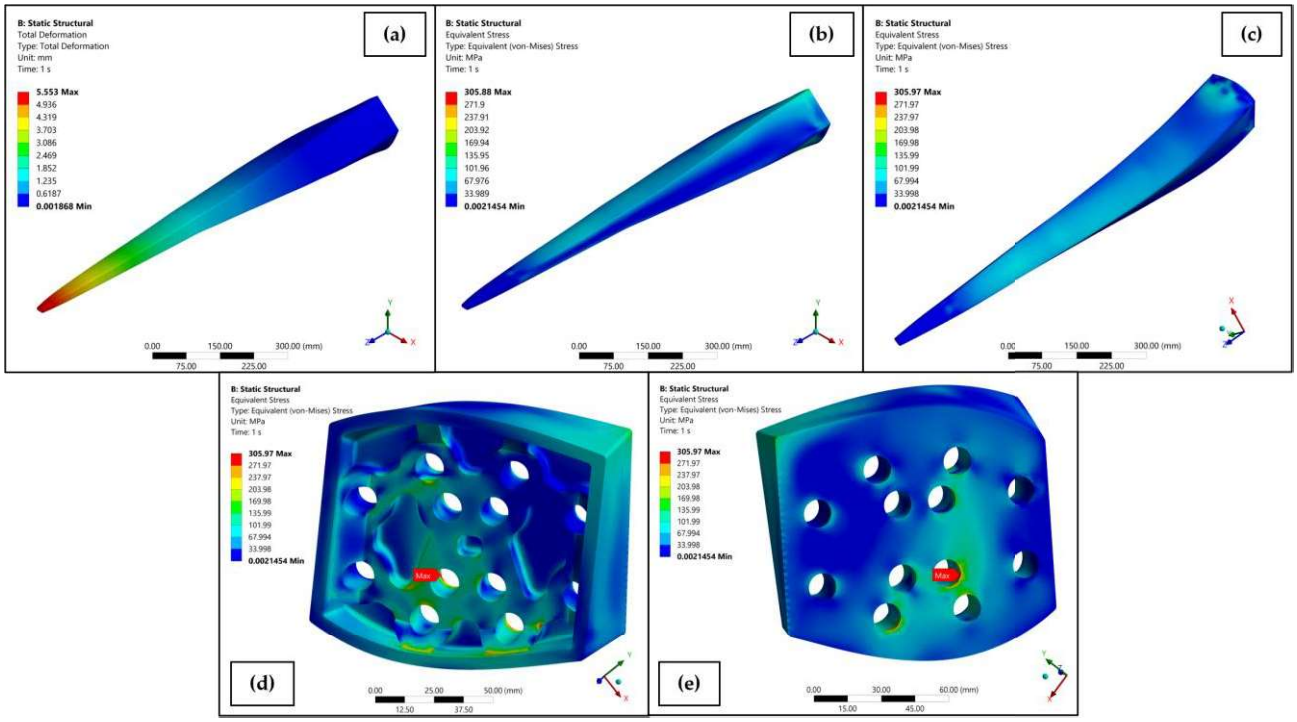

Fig. 9. **(a)** Total deformation (mm), **(b)** Low-pressure surface stresses (MPa), **(c)** High-pressure surface stresses (MPa), **(d)** Root stresses inside (MPa), **(e)** Root Stresses outside (MPa).

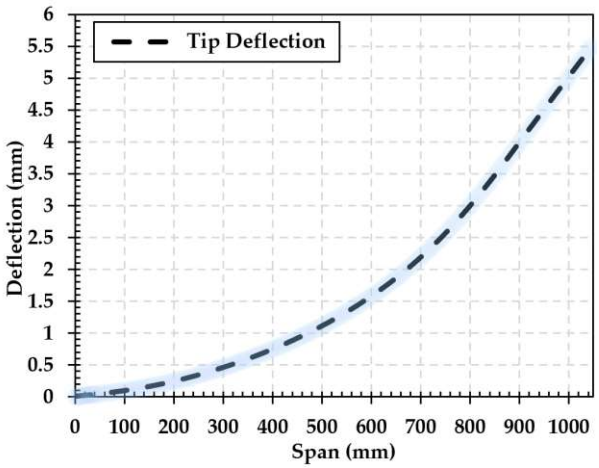

Fig. 10. Spar spanwise total deformation.

connections and reduced stress concentrations, and thereby enhanced the overall structural stability of the design. The root section was consciously designed to be broad enough to securely fit both mounting bolt patterns, resulting in an initially wider cross section that progressively tapers toward the tip. Additionally, the placement of the spar cross section within the blade geometry was engineered to transition gradually from 40% to approximately 30% chord across the span.

B. Finite element analysis

Finite element analysis (FEA) is a powerful computational tool that provides a detailed view of how complex structures behave under load. It allows engineers to predict and analyze potential areas of stress concentration, deformation, and stability issues such as buckling in structures, thus facilitating the mechanical characterization of multiple designs without having to test each one. The versatility and high-resolution insight of FEA make it an invaluable tool in the design and analysis of complex dynamic structures, such as those commonly found in MHK devices.

In this study, a finite element model of the spar was constructed. Because the whole blade surface has not been used in this instance, the pressure loads produced from the static CFD analysis could not be properly applied to the model. Therefore, the bending moment distributions were simplified even further to three-point loads along the span of the spar. These three-point loads were evenly distributed across the span, and the magnitudes were chosen to match the bending moment distribution as closely as possible (see Fig. 2). This analysis aimed to ascertain maximum stress concentrations, deformations, and eigen buckling conditions throughout the blade in response to the applied forces. Figs. 7 and 8 depict the model setup and the root connection design, respectively. Fig. 7 illustrates the three-point load application at 0.3 m, 0.6 m, and 0.9 m from the root, while Fig. 8 presents a cross section of the spar near the root, showcasing the interior design and highlighting (in green) the bolts used to connect the spar to the back plate for analysis. For consistency with future modeling efforts by Sandia on the full blade model, this model was run with the spar attached to the fixture at the 50% chord location at the root.

Upon completion of the analysis, deformations and equivalent stress were evaluated to identify any potential design weaknesses or yield areas. We observed a maximum tip deflection of 5.5 mm (0.5% of the span) (see Fig. 9(a) and Fig. 10), a level deemed acceptable for performance purposes. Equivalent stresses throughout the span remained well below yield values, generally staying

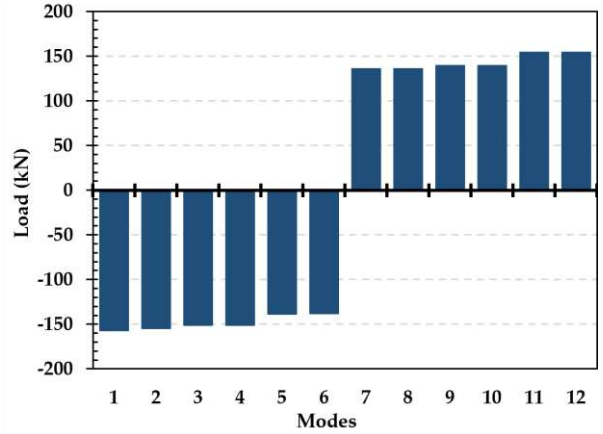

Fig. 11. Calculated buckling modes and loads from a single point load at the tip of the spar.

below 100 MPa ($< 0.3\sigma_y$), as can be appreciated in Fig. 10. (b) and (c). Highly localized stress concentrations nearing or even reaching the yield stress were identified in some corners, edges, and bolt connections at the root (Fig. 9(d),(e)). To alleviate these concentrations on edges and corners, fillets and chamfers were added. The high-stress concentrations around the bolt connections were not considered representative of real-world behavior because, in a physical test context, washers would be included, and the bolts would be pretensioned to distribute loads more evenly.

To verify structural stability under the given loads, an eigen buckling analysis was subsequently performed. For easier interpretation of the results, a 1 N load was applied at the tip, and eigenvalues were scaled accordingly. Therefore, the eigenvalues could be taken as the tip loads required to induce the computed buckling modes, shown in Fig. 11. These ranged from 130 to 150 kN, rendering the risk of buckling highly unlikely, as the spar would certainly yield before such loads were ever reached. However, the analysis did indicate that, in the unlikely event of buckling, it would occur further outboard, approximately 0.9 m from the root.

IV. Final Manufacturing

The structural blade spar was manufactured by Ai-Build with a Meltio wire laser metal deposition (LMD) printer mounted to a Kuka robotic system, using Ai-Build's AiSync software.

The part was printed without the root mounting holes, to not disrupt the tool paths of the print and consequently the homogeneity of the root reinforcement structure. The root mounting holes were to be drilled and tapped afterwards. The part was printed with a planar slicing approach, with double walls and 100% infill. No stock was added to the part, aside from three layers (3.6 mm) at the base to provide additional material for removal of the build plate. Fig. shows the tool paths generated by the AiSync software at various cross sections along the span of the spar. The part was printed using a spool of 1 mm diameter 316L SS wire with Meltio's suggested processing

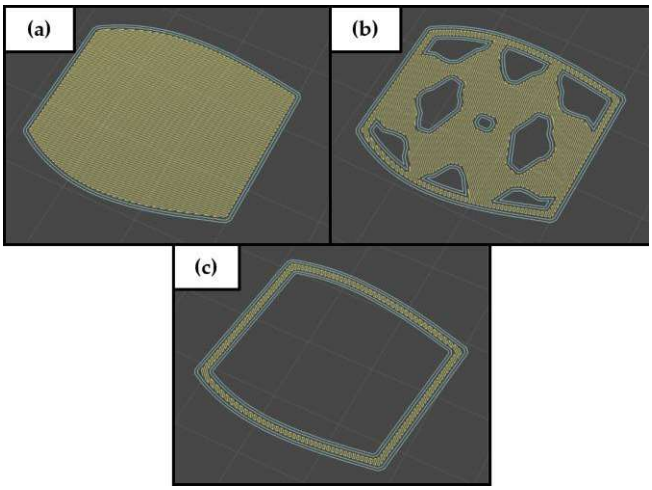

Fig. 12. Toolpaths generated by the AiSync software for the (a) base, (b) root reinforcement, and (c) box spar sections (c).

TABLE V
PRINTING PROCESS PARAMETERS RECOMMENDED BY MELTIO FOR 316L STAINLESS STEEL

Parameter	Printer Setting	Units
Layer height	1.2	mm
Layer width	1	mm
Robot speed	450	mm/min
Feeder speed	11.46	mm/s
Laser power	1100	W
Energy density	122	J/mm^3

parameters to produce fully dense parts (see Table V). Overall, the quality of the resulting spar was excellent, especially for a unique structure and perhaps the largest of its kind for marine current energy conversion (see Fig. 13).

However, some surface defects were present. This is a common issue when scaling up any AM process, especially DED [7,10]. Some surface defects were observed in areas where overhangs were present and presented themselves as waviness on the interior and exterior surfaces (see Fig. 14). This was primarily due to the molten steel sagging from insufficient support below. In the future, several strategies could be employed to minimize the likelihood of these defects, such as reducing layer heights in those areas, reducing the laser power at the outer walls, or manipulating the part orientation during printing—an additional capability of the Meltio/Kuka/AiSync system that was not utilized for this project.

The printed part also presented considerable surface defects toward the tip, in the form of excess wire fused to the surface (see Fig. 14(d)). The main cause of this was excess heat. As the cross section tapers toward the tip, the time between layers was lessened, and therefore the part had less time to cool between subsequent layers. Increasing wait times between layers could alleviate this. The concentration of wire on one side of the part also indicates that the lasers on that side may have slowly lost calibration toward the end of the print.

When complete, the outer surfaces of the spar were cleaned up and smoothed with a wire wheel and flap disc

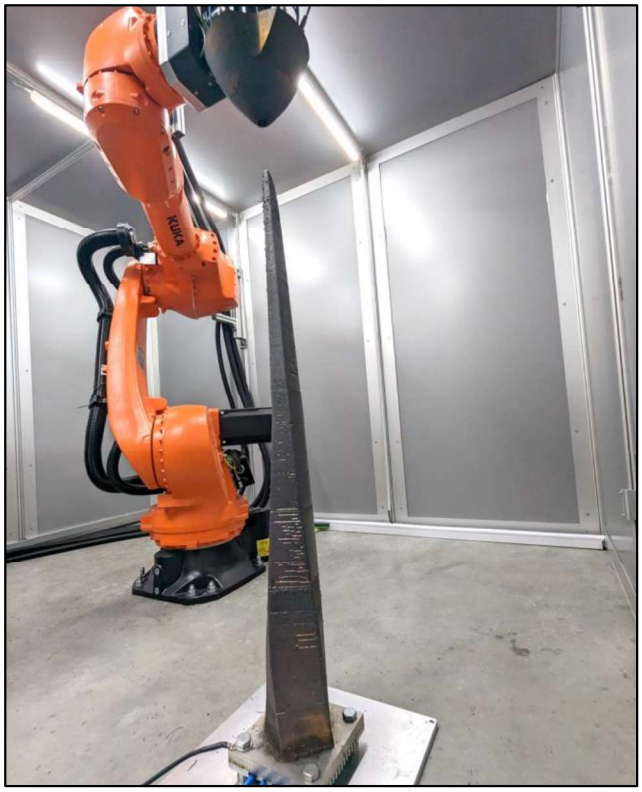

Fig. 13. The structural box spar print, complete with the Kuka/Meltio LMD system (photo by Phil Barden, Ai-Build).

on an angle grinder. It is anticipated that the surface defects will have little to no effect on the structural performance of the spar, especially around the overly conservative tip section, due to bead width limitations. If this blade spar were to be deployed, it would need to be coated to fill in the discontinuities and optimize the hydrodynamic surfaces for performance while also protecting the steel from the corrosive marine environment and biofouling.

The final defect observed was warpage of the 20 mm thick build plate at the base, when removed from its mounts. This indicates considerable residual thermal stresses within the root reinforcement, and removal of the base plate will be more challenging than originally anticipated. In hindsight, the thick plate-like reinforcement approach to the spar root was not optimal for the LMD AM process. Future designs will adopt vertical web-like reinforcements to minimize residual thermal stresses and associated warpage. Additionally, resources should be directed toward computationally modeling the printing process' resulting residual thermal stresses and distortion.

An aluminum clamping fixture was designed to match specific cross sections of the spar, so the base plate could be CNC-milled away, leaving a flat root face perpendicular to the spanwise direction (see Fig. 15). The same fixture was also used to drill and tap the root mounting points using a horizontal mill. Prior to design of the fixture, cursory measurements of the spar cross sections were taken and indicated that the root was the only region that experienced considerable distortion. Also, point

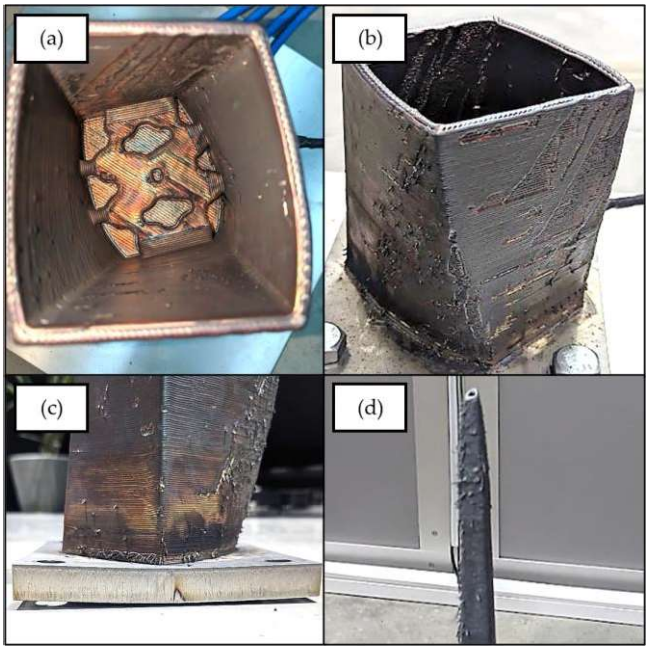

Fig. 14. Defects observed in the final print: (a) interior waviness, (b) exterior waviness, (c) base plate warpage, and (d) excess wire at the tip (photos by Phil Barden (Ai-Build) and Paul Murdy (NREL)).

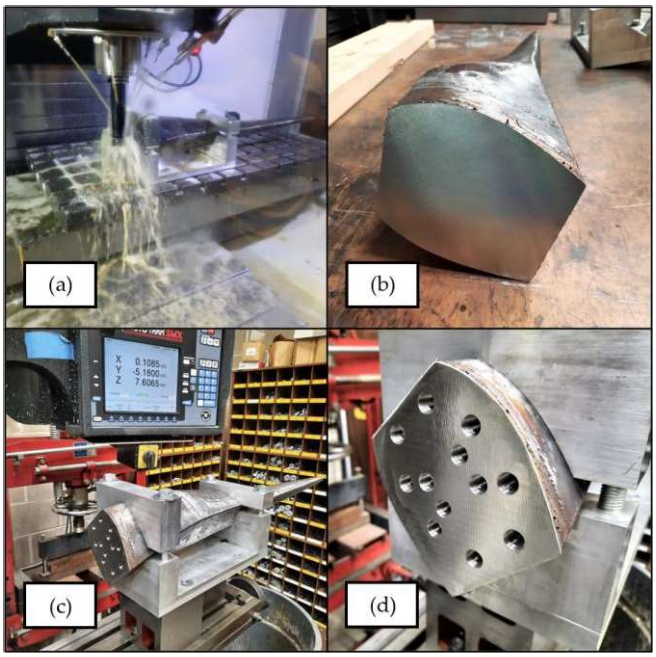

Fig. 15. The final machining steps to complete the spar: (a) base plate removal, (b) the resulting flat root surface, (c) drilling and tapping the root mount holes, and (d) the final completed root face (photos by Paul Murdy (NREL)).

measurements of the base plate distortion indicated that it would be feasible to remove the base plate and mill the root flat, while still maintaining the as-designed thickness of the root reinforcement at a minimum, due to the additional three layers that were included in the print. The base plate was successfully removed with no additional warping observed. The flatness was measured to within 0.025 mm. Now that the final machining processes are complete, the spar will be mounted to a test stand and subjected to a rigorous structural validation program. Prior to testing, the final spar geometry will be measured

using a laser scanning system and compared to the original designed geometry.

V. Conclusions and Continued Research

This study has successfully established a simple, reliable design process for an open-source MHK blade structural component manufactured using AM, broadening the horizons for MRE technologies. By leveraging the flexibility and precision of finite element modeling, this work expedited the design improvement process, minimizing the need for potentially time-consuming trial and error. This approach allowed for the efficient incorporation of real-world constraints to our design, helping improve design features and reducing the development time.

The challenges and limitations of the scoped printing processes (scalability) and materials (availability and durability) were assessed within the marine environment context, narrowing the decision to the DED process and 316L SS for the spar. The use of DED, a technology commonly associated with the aerospace industry, was introduced for the development of complex marine structures, resulting in the manufacture of a full-scale structural spar that twists, tapers, and shifts chordwise continuously through its span while also following the low- and high-pressure surface geometries of the MHKF1 turbine blade. The resulting geometry was a singular component that could not be easily replicated with conventional manufacturing approaches. The printing process was carefully laid out, highlighting surface finish issues due to insufficient supports and excess heat accumulation, and warping effects at the root due to residual thermal stresses, defects which are inherent to the current state of most current DED technologies. These lessons learned will certainly be beneficial to future iterations of 3D-printed MRE structural components.

Future work will focus on structurally validating the FEA models constructed through this research. Representative static and dynamic loads will be applied to the spar and replicated in the FEA models. Integration of leading- and trailing-edge hydrodynamic fairings will be explored by developing models that apply the actual pressure loads from the CFD analysis. The components will then be produced using FDM to complete the full MHKF1 blade geometry. This would allow the spar to function as the blade's main load-bearing component, pushing the boundaries of what is currently achievable in MRE technologies for fast, affordable, and reliable blade structural design and implementation for rapid testing of MRE technologies.

In summary, this research serves as a unique benchmark study, leading to new waters in the exploration and expansion of MRE technologies. By successfully developing and applying advanced AM techniques in the marine energy sector, this work contributes to the further anchoring of MRE's position in the clean energy landscape. The outcomes of this work are expected to reverberate throughout PBE initiatives, underlining the potential of advanced manufacturing technologies to revolutionize MRE, and making a significant step toward a more sustainable future.

Acknowledgements

The authors would like to thank those whose contributions have been invaluable in the realization of this project. We are grateful to Dr. Thanh Toan Tran (NREL) for his work on the CFD loads analysis, to Scott Hughes, Senu Sirnivas, and Amanda Morton (NREL) for their continued support and insightful feedback throughout the project, and finally to the team at Ai-Build and Nick Johnson from One Off Robotics whose technical support was indispensable in the manufacturing of the spar.

References

[1] LiVecchi, A., A. Copping, D. Jenne, A. Gorton, R. Preus, G. Gill, H. R. Green, S. Geerlofs, S. Gore, D. Hume, W. McShane, C. Schmaus, and Spence, "Powering the Blue Economy; Exploring Opportunities for Marine Renewable Energy in Maritime Markets.," Washington, D.C., 2019.

[2] P. Murdy, J. Dolson, D. Miller, S. Hughes, and R. Beach, "Leveraging the advantages of additive manufacturing to produce advanced hybrid composite structures for marine energy systems," Appl. Sci., vol. 11, no. 3, pp. 1–15, 2021.

[3] F. Caviggioli and E. Ughetto, "A bibliometric analysis of the research dealing with the impact of additive manufacturing on industry, business and society," Int. J. Prod. Econ., vol. 208, no. December 2018, pp. 254–268, 2019.

[4] A. A. Fontaine, W. A. Straka, R. S. Meyer, M. L. Jonson, S. D. Young, and V. S. Neary, "Performance and wake flow characterization of a 1:8.7-scale reference USDOE MHKF1 hydrokinetic turbine to establish a verification and validation test database," Renew. Energy, vol. 159, pp. 451–467, 2020.

[5] Neary, V., "An Instrumented Reference Hydrokinetic Turbine System for Load Response Characterization at a Tidal Energy Test Site", vol. 2021, 2021.

[6] L. Hitzler, M. Merkel, W. Hall, and A. Öchsner, "A Review of Metal Fabricated with Laser- and Powder-Bed Based Additive Manufacturing Techniques," Advanced Engineering Materials, vol. 20, no. 5. pp. 1–28, 2018.

[7] A. Suárez, F. Veiga, T. Bhujangrao, and E. Aldalur, "Study of the Mechanical Behavior of Topologically Optimized Arc Wire Direct Energy Deposition Aerospace Fixtures," J. Mater. Eng. Perform., vol. 31, no. 8, pp. 6270–6282, 2022.

[8] F. Froes, R. Boyer, and B. Dutta, "Introduction to aerospace materials requirements and the role of additive manufacturing," Addit. Manuf. Aerosp. Ind., pp. 1–6, 2019.

[9] C. H. Shiau et al., "Deformation behavior and irradiation tolerance of 316 L stainless steel fabricated by direct energy deposition," Mater. Des., vol. 204, p. 109644, 2021.

[10] D. Svetlizky et al., "Directed energy deposition (DED) additive manufacturing: Physical characteristics, defects, challenges and applications," Mater. Today, vol. 49, no. October, pp. 271–295, 2021.